3D Point Measurement from Space using TerraSAR-X HS and ST Stereo Imagery

WOLFGANG KOPPE[1], SIMON D. HENNIG[1] & LAURA HENRICHS[1]

Zusammenfassung: Der auf TerraSAR-X basierte Ansatz zur Erfassung von 3D Bodenpasspunkten ist besonders für unzugängliche, abgelegene Gebiete oder Regionen interessant, in denen die Erhebung von terrestrischen Informationen nicht möglich ist..Basierend auf TerraSAR-X Stereo-Bilddaten aus verschiedenen Blickwinkeln werden hochgenaue Passpunkte der Erdoberfläche extrahiert. Dafür werden hochaufgelöste Daten im High Resolution SpotLight (HS) and Staring SpotLight (ST) Mode verwendet. Besonders der ST Mode mit seiner Sub-meter Auflösung und hoher Radiometrischer Genauigkeit ermöglicht die Messung von Bodenpasspunkten im Sub-meter Bereich. In der vorliegenden Studie werden HS und ST Daten für die Bodenpasspunktgewinnung analysiert und die Genauigkeiten ermittelt.

1 Introduction

Commercial TerraSAR-X Services started in January 2008, following the launch of the first spacecraft in June 2007. The second spacecraft, namely the TanDEM-X satellite, was launched in June 2010. The X-Band SAR sensors provide images with a spatial resolution up to three meters for StripMap and less than one meter for very high resolution imagery (FRITZ & EINEDER 2014).

Reliable Ground Control Points (GCPs) are an essential input for the precise orthorectification of remote sensing imagery, the exact location of targets or the accurate georeferencing of a variety of geo-datasets. Inadequate co-registration makes the merging, the comparison and generally the co-processing of the data impossible. Although GCPs collected by terrestrial means typically offer a high accuracy, the TerraSAR-X based spaceborne approach is of significant interest in areas where access can be hazardous or may not be authorized. Thanks to TerraSAR-X's high orbit accuracy (centimeter range), the precise radar beam tracing, its high resolution and the resulting high location accuracy of the imagery (EINEDER et al. 2011), the satellite proves to be highly suitable for obtaining 3D ground information. Based on stereo imagery or multiple image datasets, GCPs can be obtained with high accuracy in East (E), North (N) coordinates and in Height (H). The subsequent utilization of the retrieved points is to establish a control point database, particularly in poorly mapped areas, where such information is not available or insufficiently accurate. The focus of this study is the quality assessment of the retrieved 3D coordinates. To achieve this, a comprehensive test strategy was conducted to validate the accuracy of retrieved 3D point coordinates.

Since end of 2013, TerraSAR-X and TanDEM-X are operated with a new sub-meter acquisition mode, the Staring SpotLight (ST) mode. In general, Synthetic Aperture Radar (SAR) spotlight

[1] Airbus Defence and Space, Geo-Intelligence, Claude Dornier Straße, 88090 Immenstaad, Germany; E-Mail: [wolfgang.koppe, simon.hennig, laura.henrichs]@astrium.eads.net

modes are characterized by azimuth antenna steering to a rotation center. The difference to a classical sliding SpotLight mode is the location of the rotation center inside the image scene and the larger steering angle range of ±2.2° (MITTERMAYER et al. 2012). The larger steering range provides an improved azimuth resolution, which enhances image resolution and radiometric performance. This new dimension of commercially available very high resolution SAR data opens up new possibilities in geodetic surveying from space.

2 GCP Extraction Method from TerraSAR-X Stereo Imagery

TerraSAR-X and TanDEM-X are capable of high resolution and multi-beam image acquisition. Along with the image data, detailed and very precise orbit data allow for highly accurate 3D information extraction based on stereo or multi-angle image data sets. The image geolocation positioning error is proved to be less than 10 cm in azimuth and range (EINEDER et al. 2011).
For ground control point extraction, a minimum of two images from the same orbit direction or, ideally, from ascending and descending orbits are acquired of the area of interest. For high accuracy point measurement from space, the intersection angle α between the input images is of great importance for a stable geometric model. Detailed analysis of image stereo constellations for high performance can be found in KOPPE et al. (2012) and RAGGAM et al. (2010).

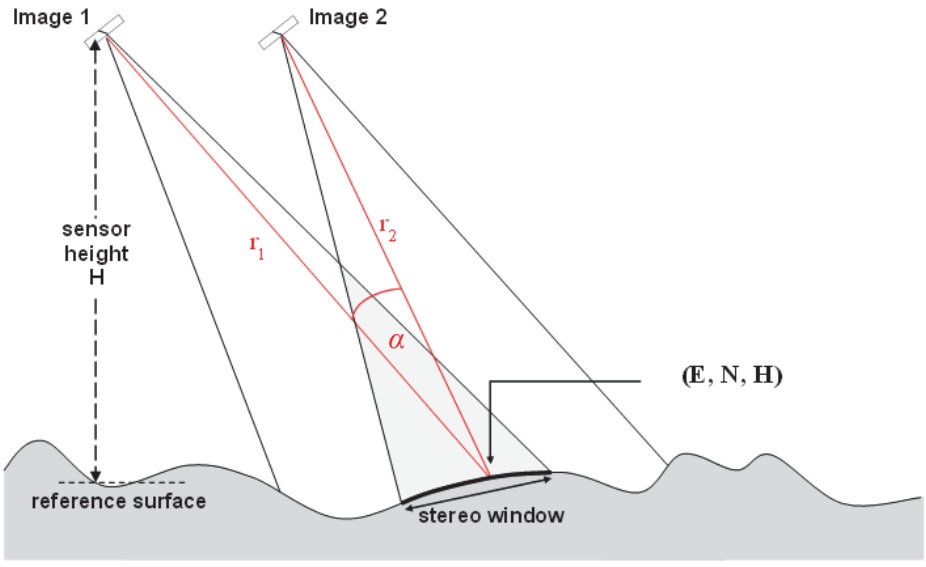

Fig. 1: Stereo image constellation from one orbit direction for GCP extraction. r is the range distance, E, N, and H the East, North and height.

Manual point measurements of corresponding points made in two or more images are used to determine the ground coordinates (E, N, H). The calculation of the ground coordinates based on the point measurements is called spatial point intersection. The simple case of two input images from the same orbit direction is depicted in Figure 1. Image 1 and 2 are the input stereo images, r_1 and r_2 are the range distances to the point of interest within the stereo window. The general mathematical background of this intersection procedure is given in RAGGAM & ALMER (1990).

During this procedure, two or more range cycles are intersected in space and thus it is based on the SAR Doppler and range equations. These two equations are applicable to each individual point measurement. Consequently, four equations are available if a point is measured in a stereo pair, which can be further used to determine the three ground coordinates (E, N, H). This over-determined system of equations – four equations in order to determine three unknown coordinates - is solved by the least squares procedure.
Each additional point measurement, made in further available images, yields another two equations and thus to an increased over-determination. The point intersection then becomes more robust and the result of the intersection is more precise than in the standard stereo mapping procedure based on two images only. The detailed mathematic algorithm for the least squares solution can be found in RAGGAM & ALMER (1990). The point selection process, especially of strong scatterers in radar imagery such as metallic pylons, is supported by local oversampling (cubic spline) to determine exactly the scattering center in subpixel accuracy. Figure 2 shows a point scatterer in the original SAR image (left) and after local oversampling (right) for subpixel point scattering center determination.

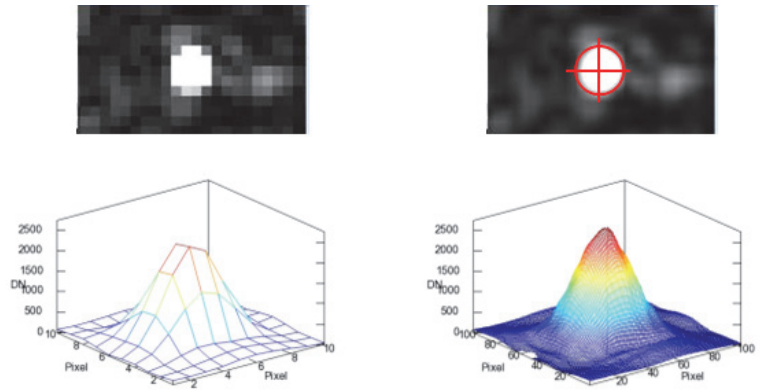

Fig. 2: Point scatterer image and digital number plot in unprocessed SAR image (left) and after local oversampling (right) for subpixel point selection.

2.1 Theoretical Error Sources of Retrieved 3D Coordinates

Two main error sources must be taken into account when assessing the accuracy of the 3D coordinates. The first is the inherent system error and the second is the error introduced during the manual point selection process. System errors are summarized in three categories: orbit precision, path delay of signal due to ionosphere and troposphere variations and solid Earth tides. The orbit accuracy for the most precise orbit option, the science orbit, is calculated with an accuracy of around 20 cm (3D, 1 sigma), aiming at 10 cm in range and azimuth (FRITZ & EINEDER 2014). The path delay due to atmospheric effects can be corrected by GPS TEC maps, which reduces the traveling time error to single-digit centimeter range. The solid Earth tides are also in centimeter range and can be corrected by a solid Earth tide model. The range and azimuth error due to system inaccuracies is summed up to less than 10 cm.
Compared to the controlled system error sources, the second operator introduced error is more severe. As the homologous point has to be selected in all the input images, the target has to be

clearly visible in all of the images. An error in one of the images causes an error in the range circles intersection. The impact of selection error is followed by the shifting of at least one range circle and can be expressed as:

$$D = \Delta r / \sin \Delta\theta \qquad (1)$$

where D is the resulting 3D error, Δr the measured range error and $\Delta\theta$ the intersection angle between the stereo images. The dependence on the incidence angle difference of the stereo images is evident according to equation 1. To optimize the geometric model, data from ascending and descending orbit directions is used to approximate the ideal geometric intersection condition of $\Delta\theta \sim 90°$.

3 TerraSAR-X Input and Reference Data

3.1 TerraSAR-X Input Data

The test site selected to be investigated was an area South-West of Denver, USA, covering mainly urban/suburban and rural areas. According to the image data acquisition scenario shown in Figure 1, stereo imagery from High Resolution SpotLight (HS) and Staring SpotLight (ST) modes in HH polarization was acquired. For each measurement campaign, three images from different orbit directions were chosen. The image parameters are summarized in Table 1. As the images were acquired at different times, only the stable points were measured in the 2014 ST and compared to the 2011 HS data. Two images of each data stack were acquired in the same orbit geometry. Due to acquisition constraints, image 5 could not be acquired with the same parameters as image 1. An additional HS image (ID 7) was taken as the first three images were acquired during winter time, which could influence the radiometric performance of the image.

Tab. 1: Summary of acquired test data in High Resolution SpotLight (HS) and Staring SpotLight (ST) modes (rg - range, az - azimuth).

ID	Acquisition Mode	Date	Orbit Direction	Incidence Angle [°]	Resolution rg/az [m]
1	HS	19.02.2011	Ascending	48.8	1.00 / 1.14
2	HS	25.02.2011	Ascending	35.8	1.02 / 1.14
3	HS	28.02.2011	Descending	42.5	0.99 / 1.15
4	ST	09.05.2014	Descending	42.5	0.88 / 0.38
5	ST	15.05.2014	Descending	53.5	0.74 / 0.32
6	ST	08.06.2014	Ascending	35.8	1.03 / 0.44
7	HS	07.10.2014	Ascending	35.8	1.03 / 1.14

In Figure 3, an overview of the Denver test site and measured points is shown. Points are selected in urban and suburban areas. To achieve a mix of diverse features, different elements such as point scatterers (lightning pole and power pole), road crossings and roundabouts were chosen.

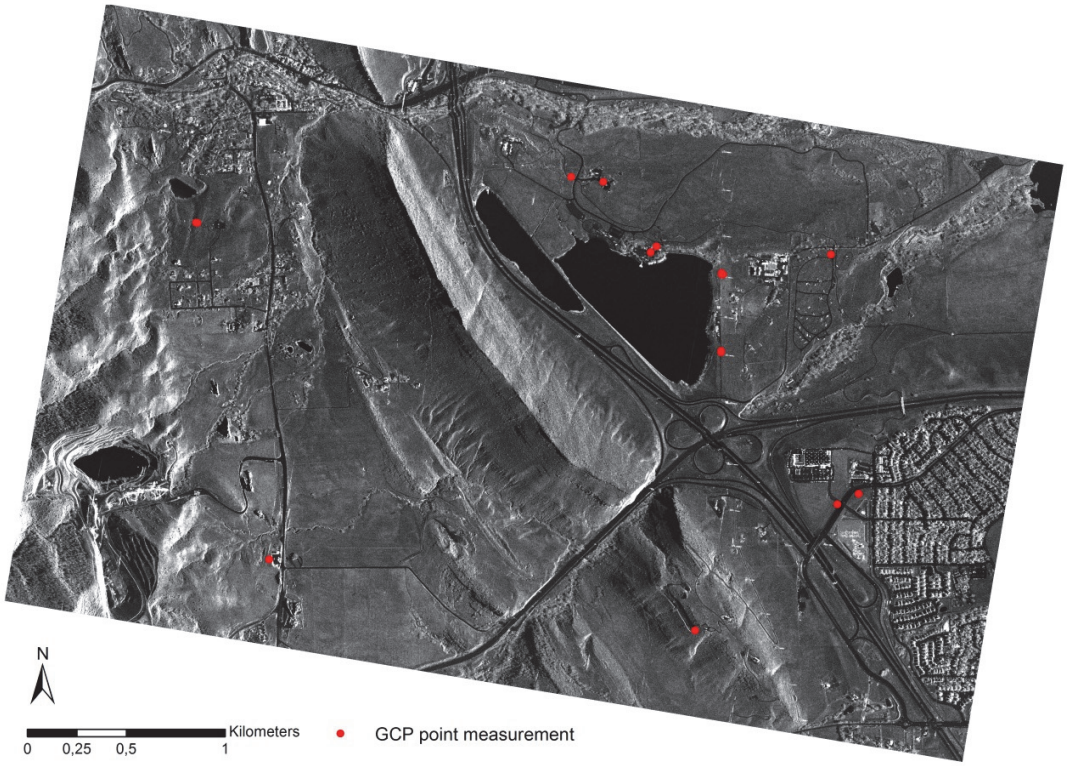

Fig. 3: Overview of Area of Interest and selected points for ground coordinate measurements.

3.2 Reference Data

For the validation of Ground Control Points measured from TerraSAR-X imagery, highly accurate coordinates of features obtained by GPS observations were used. The advantages of these measurements are the very high accuracy of the measurements and the global availability in a consistent quality. For this analysis, the ITRF 2008 with the Epoch of 2012.0 was applied providing the consistent reference for comparison. The coordinates of the GCPs were measured with survey grade GPS equipment and processed to an absolute and global accuracy better than 10 cm with CE95 and LE95 confidence levels (HUMMEL 2014).

4 GCP 3D Accuracy of TerraSAR-X HS and ST

To attain the final accuracy of the retrieved GCP points, system and manual introduced errors are contributing sources as described in section 2.1. As system errors can be neglected, the main error source remains the point selection capabilities, which is dependent on image resolution and radiometric performance. In section 4.1, the input images HS and ST are compared with regard to resolution and radiometric performance for point selection. In section 4.2, the measured GCPs are compared to ground truth information (GPS measurements) described in section 3.2.

4.1 Point Selection Capabilities of HS and ST

Figure 4 depicts the different backscatter response of a point target in HS and ST image. Based on the higher resolution and better radiometric performance of ST, the point target is clearly pronounced. This is particularly important for smaller point targets with lower backscatter intensity. Due to this, more point targets can be found in ST imagery as a ground control source.

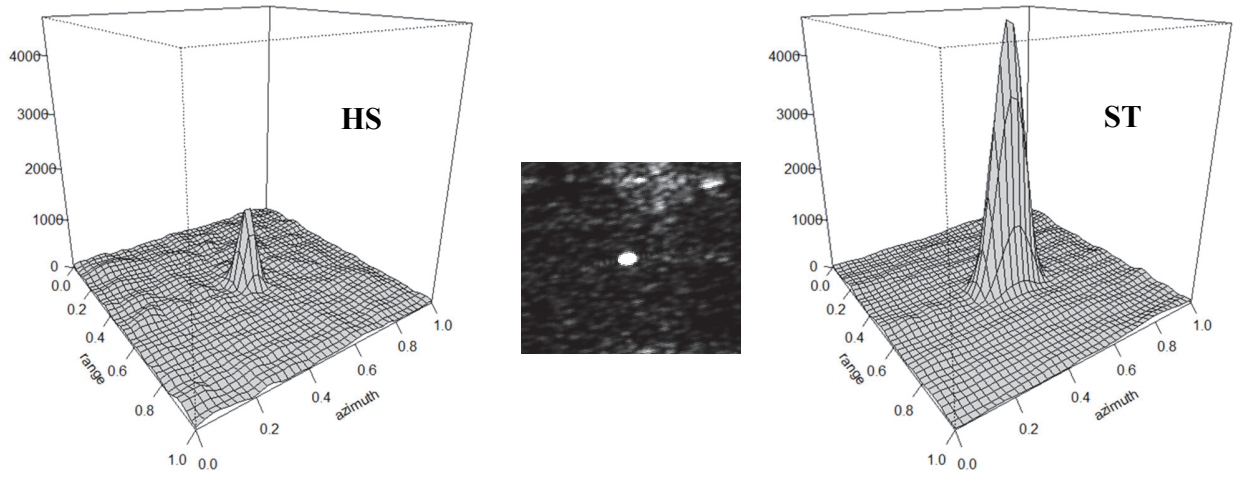

Fig. 4: Signal response of a point target (middle) in the HS (left) and the ST image (right).

Fig. 5: Zoom of HS and ST mode for various measured points.

Furthermore, Figure 5 shows a close-up of the same area in HS and ST mode; two images of HS with different weather conditions. All have been multi-looked to a resolution of 1m×1m. The HS images are noisier and the streets are not clearly separable from the surrounding rough surface, whereas in the ST image the road clearly stands out. This radiometric resolution improvement of the ST image is an important advantage for the ground control point selection process of non-point targets such as road crossings or surface type differences.

4.2 Statistical Analysis of GCP Measurements

The 3D accuracy analysis is based on the comparison of retrieved GCP coordinates with the measured GPS measurements. The RMSE values of the point residuals in East (ΔE), North (ΔN) and height (ΔH) as well as for horizontal are calculated and plotted in a 2D diagram. Table 2 summarizes the RMSE values for HS and ST input images. Analyzing the accuracy values in Table 2 and Figure 6, the following results can be formulated:

- HS and ST results are in the specified value range of GCP product
- There is a clear RMSE accuracy improvement in the planimetric direction East and North of ST input imagery by approximately 40%
- The height accuracy values of HS and ST are in the same range
- The final 3D accuracy improved by approximately 30% from 1.27m RMSE for HS to 0.85m RMSE for ST

The RMSE residuals in azimuth (N) and range are in the order of 2 pixels, while the RMSE horizontal residual length is in the order of 2-3 pixels for HS and ST. Note that pixel spacing for HS is 50cm and for ST approximately 20cm. This corresponds with the estimated point identification and measurement accuracy dependent on resolution and image radiometry.

Tab. 2: Absolute 3D geolocation accuracies for the different measured features (n=12).

Acquisition Mode		ΔE [m]	ΔN [m]	ΔH [m]	Δ Horizontal [m]	Δ Spatial [m]
HS	Mean	-0.13	-0.27	-0.24	1.10	1.21
	RMSE	**0.80**	**0.87**	**0.48**	**1.18**	**1.27**
ST	Mean	-0.28	-0.39	-0.07	0.68	0.83
	RMSE	**0.48**	**0.54**	**0.44**	**0.73**	**0.85**

In Figure 6, the horizontal residuals of the 12 single measurements, based on HS and ST, are plotted in a 2D diagram. In the HS plot, six points are within the 1m-radius and 11 of 12 points are within the 2m-radius. Compared to this, 11 of 12 points of the ST plot are within the 1m-radius. Although the absolute horizontal accuracy values of HS and ST are closely in the range of 1m RMSE, the HS residuals are more widely spread within the plot and the ST residuals are in a smaller *x* and *y* range around the point of origin.

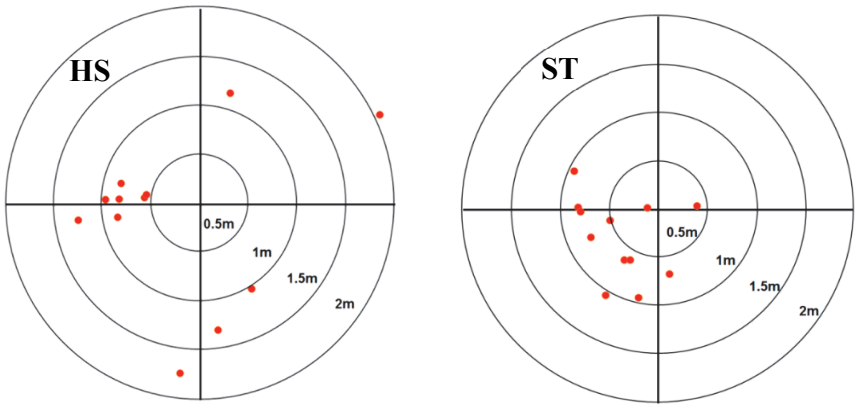

Fig. 6: 2D residual plots of HS and ST measurements.

5 Conclusion

The recent study has shown that TerraSAR-X derived Ground Control Points can be measured with accuracy up to 1m (RMSE, 3D vector) under optimized stereo disposition and with high resolution SAR imagery. Since the 3D accuracy is strongly dependent on the disparity angle, stereo constellation and over-determination (more than two input images), an optimized acquisition constellation should be used for GCP retrieval. According to the error budget estimation, the main error of the overall error budget is contributed by manual selection of the corresponding pixel in the different images due to image resolution and radiometric limitations. For point selection is very important to have best resolution and radiometric performance to optimize the selection process. The TerraSAR-X ST image mode provides significant higher azimuth resolution and radiometric performance. Due to the increased compression gain, there is a gain in the detectability of point targets (about 7dB) in the full resolution ST data which improves especially the manual selection of point targets.

6 References

EINEDER, M., MINET, M.C., STEIGENBERGER, P., CONG, X. & FRITZ, T., 2011: Imaging Geodesy – Towards Centimeter-Level Ranging Accuracy With TerraSAR-X. IEEE Transactions on Geoscience and Remote Sensing **49** (2), S. 661-671.

FRITZ, T. & EINEDER, M., 2014: TerraSAR-X Basic Product Specification Document. TX-GS-DD-3302, Issue 1.9, http://www.geo-airbusds.com/en/228-terrasar-x-technical-documents (accessed December 2014).

HUMMEL, P., 2014: Remotely sensed ground control points. White paper by CompassData Inc., http://www.compassdatainc.com (accessed December 2014).

KOPPE, W., WENZEL, R., HENNIG, S., JANOTH, J., HUMMEL, P. & RAGGAM, H., 2012: Quality assessment of TerraSAR-X derived ground control points. IEEE International Geoscience and Remote Sensing Symposium (IGARSS), S. 3580-3583.

MITTERMAYER, J., WOLLSTADT, S., PRATS, P., SCHEIBER, R. & KOPPE, W., 2012: Staring Spotlight imaging with TerraSAR-X. IEEE International Geoscience & Remote Sensing Symposium(IGARSS), S. 1606-1609.

RAGGAM, H. & ALMER, A., 1990: Mathematical Aspects of Multi-Sensor Stereo Mapping. Proc. of 10th Annual IGARSS Symposium: Remote Sensing - Science for the Nineties **3**, S. 1963-1966.

RAGGAM, H., PERKO, R., GUTJAHR, K.-H., KOPPE, W., KIEFL, N. & HENNIG, S., 2010: Accuracy Assessment of 3D Point Retrieval from TerraSAR-X Data Sets. EUSAR 2010, 8th European Conference on Synthetic Aperture Radar, Aachen, 07-10 June 2010.